COMPDYN 2013
4th ECCOMAS Thematic Conference on
Computational Methods in Structural Dynamics and Earthquake Engineering
M. Papadrakakis, V. Papadopoulos, V. Plevris (eds.)
Kos Island, Greece, 12–14 June 2013

CHARACTERIZATION OF THE INFLUENCE OF RAIL WEAR ON TRAIN DYNAMICS

Nicolas Lestoille[1,2], Guillaume Perrin[1,2,3], and Christine Funfschilling[2]

[1]Université Paris Est, Modélisation et Simulation Multi-Echelle (MSME UMR 8208 CNRS)
5 Bd. Descartes, 77454 Marne-la-Vallée, France
e-mail: {nicolas.lestoille,guillaume.perrin}@sncf.fr

[2] SNCF, Innovation and Research Department
Immeuble Lumière, 40 avenue des Terroirs de France, 75611, Paris, Cedex 12, France
e-mail: christine.funfschilling@sncf.fr

[3] Université Paris Est, Navier (UMR 8205 ENPC-IFSTTAR-CNRS)
Ecole Nationale des Ponts et Chaussées, 6 et 8 Avenue Blaise Pascal, Cité Descartes, Champs sur Marne, 77455 Marne-la-Vallée, Cedex 2, France

Keywords: Rail Wear, Railway Dynamics, Wheel-Rail Contact, Statistical Characterization of Contact.

Abstract. *The study presented here aims at characterizing the influence of the rail wear on the train dynamic response. Rail profiles have been measured on a real track and post-processed in order to be used in a mutlibody simulation of the train's response. Wear modes have been extracted from the measures with a Principal Orthogonal Decomposition (POD). The profiles have been projected on these modes, giving a good characterization of the profiles' geometry. In a second step, the train's dynamic response on the measured track is simulated with a multibody software. The result shows that wear reduces the train's stability.*

1 INTRODUCTION

Wheel-rail contact is one of the main sources of excitation of the train. The rail profile is so designed that the wheel is guided by the track and the wheel-rail contact area dissipates as few energy as possible. Then the wheel-rail contact has to guide the vehicles in the curves without any loss of stability. That is why the characterization of the wheel-rail contact is essential for a good understanding of the train dynamics.

The goal of this study is to characterize the influence of rail wear on the train's dynamic response. For this purpose, rail profiles have been measured on a real track, and the train's dynamic behavior is computed with a mutlibody software.

The first section of this proceeding will focus on the analysis of the rail profiles' geometry, projecting the measured profiles on a statistical basis. In the second section, the train's dynamic response on the measured track will be computed and analysed.

2 RAIL PROFILES ANALYSIS

2.1 Post-processing of measures of rail profiles

Rail profiles have been measured experimentally on a real track, using laser cameras fixed under the measuring train, as shown in figure 1. Profiles have been measured each 25 cm during 13 km. The first step of post-processing consists in erasing aberrant points and repositionning the rail profiles to correct the train's roll.

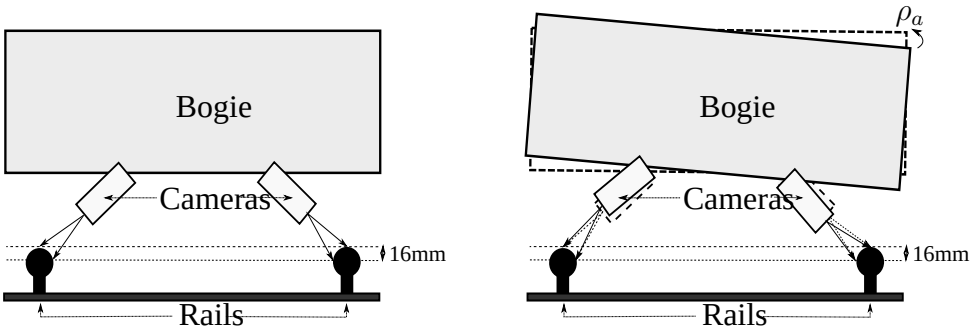

Figure 1: Experimental protocol

Then rail profiles are smoothed to remove the measurement noise. The profiles are written in polar coordinates (r, α). Since coordinates are discrete, $N_\alpha = 250$ equally distributed values of $r(\alpha)$ are taken with α in $[0.5, \pi + 0.1]$ radians (see figure 2). Finally, the profiles are sorted in low and high rails.

2.2 Stochastic characterization of rail profiles geometry

The rail profiles' radius is written as a function of the angle α in polar coordinates (see figure 2), with α in $\Omega = [0.5, \pi + 0.1]$ radians, as in paragraph 2.1. To characterize the rail wear, rail profiles are projected on a statistical basis of dimension M, obtained through a principal orthogonal development (POD) of the profiles' geometry [1] [2].

The space $\mathcal{L}^2(\Omega, \mathbb{R})$ of square integrables functions on Ω, with values in $\mathbb{R}$, is equipped with

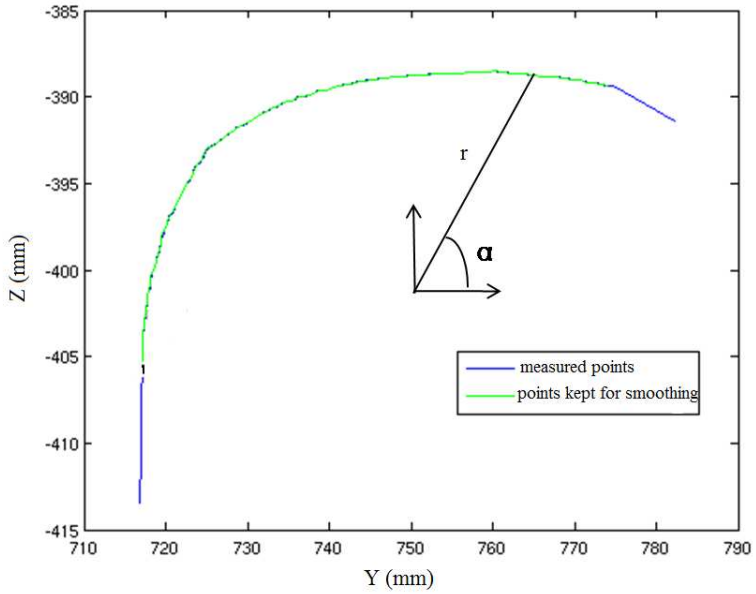

Figure 2: Measured Rail Profile

the inner product $(.,.)$, such that for all u and v in $\mathcal{L}^2(\Omega, \mathbb{R})$,

$$(u, v) = \sum_{i=1}^{N_\alpha} u(\alpha_i)v(\alpha_i). \tag{1}$$

The basis computed through the POD is composed of vectors $\{b_m(\alpha), \alpha \in \Omega\}_{1 \leq m \leq M}$, that can be seen as wear modes. They are orthonormal functions on which the rail radius is projected. The projection is denoted $\hat{r}(\alpha)$ such that, for all $\alpha \in \Omega$,

$$\hat{r}(\alpha) = \sum_{m=1}^{M} b_m(\alpha)C_m, \qquad \sum_{i=1}^{N_\alpha} b_m(\alpha_i)b_p(\alpha_i) = \delta_{mp}, \qquad C_m = \sum_{i=1}^{N_\alpha} r(\alpha_i)b_m(\alpha_i), \tag{2}$$

where δ_{mp} is the kronecker symbol that is equal to 1 if $m = p$ and to zero otherwise. The vector $\mathbf{C} = (C_1, ..., C_M)$ is a M-dimensionnal random vector.

The vector $\mathbf{C}$ is normalized, extracting its determinist norm $\sqrt{\lambda} = (\sqrt{\lambda_1}, ...\sqrt{\lambda_M})$ and computing the normalized random vector $\eta = (\eta_1, ..., \eta_M)$ such that,

$$\eta_m = \frac{(r, b_m)}{\sqrt{\lambda_m}} \qquad \forall m \in [|1, M|] \tag{3}$$

$$E\{\eta_m \eta_p\} = \delta_{mp}, \qquad \forall (m, p) \in [|1, M|]^2 \tag{4}$$

$$\hat{r}(\alpha) = \sum_{m=1}^{M} b_m(\alpha)\eta_m\sqrt{\lambda_m}, \qquad \forall \alpha \in \Omega, \tag{5}$$

where $E\{.\}$ is the mathematical expectation.

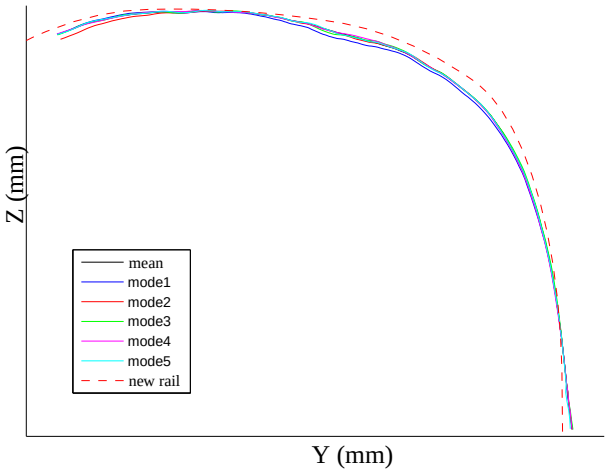

Figure 3: First modes of projection

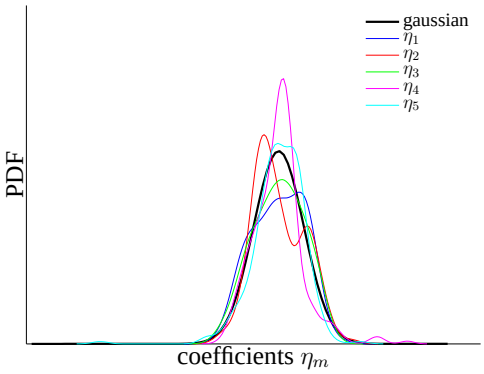

Figure 4: First coefficients η_m for the high rail

One can now observe wear modes and random wear coefficients of the projection basis. The figure 3 confirms that the modes are sorted by descending energy, because higher modes get closer of the mean profile. The first mode appears to be the one which is the most worn.

A look at the first five random coefficients η_m, with $m \in [|1, 5|]$, of the projection basis (see figure 4) gives information about the variability of the rail profiles' geometry. It can be seen that the variability is relatively low, because only high rails are here taken into account.

Nevertheless, one could suppose that wear on both rails (high and low rails) is correlated. This makes take into account rails from both track sides to compute the projection basis, in order to describe the whole track.

2.3 Analysis of the correlation between high and low rails

In order to take into account the correlation between high and low rails in the vectors of the projection basis, both rails have to be described on the same basis. For this reason, no more single rail profiles but pairs of rail profiles are studied, steming from one track section. The geometry of ν pairs of rail profiles has been measured. These experimental data are denoted by

the $\mathbb{R}^2$-vector value $\mathbf{r} = \{(r_1(\alpha), r_2(\alpha)), \alpha \in \Omega\}$ for which each component $\{r_i\}_{1 \leq i \leq 2}$ represents a rail. As in paragraph 2.2, $\mathbf{r}$ is projected on a statistical basis obtained by a POD. The vectors and the coefficients of the projection basis are represented in figure 5 and 6. It can be seen that each vector represents at the same time the high and the low rails, which confirms the assumption that high and low rails should be modeled together.

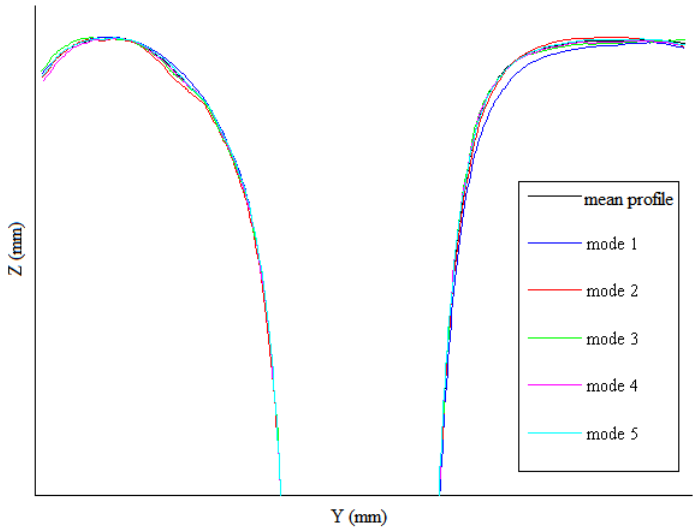

Figure 5: First modes of projection for both rails

Then the norm of each vectors is plotted in figure 7, coloring differently the part due to the high rail and the one due to the low rail. Here again, it can be seen that both high and low rails take part in the projection vectors, so that wear on both rails is highly correlated.

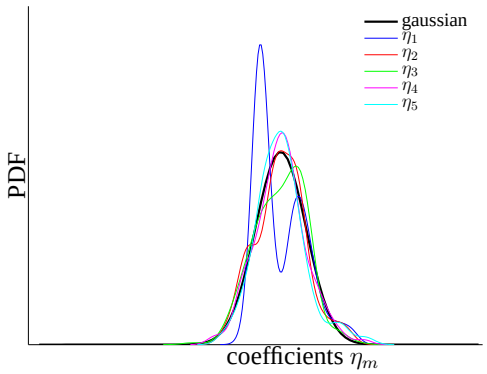

Figure 6: First coefficients η_m for both rails

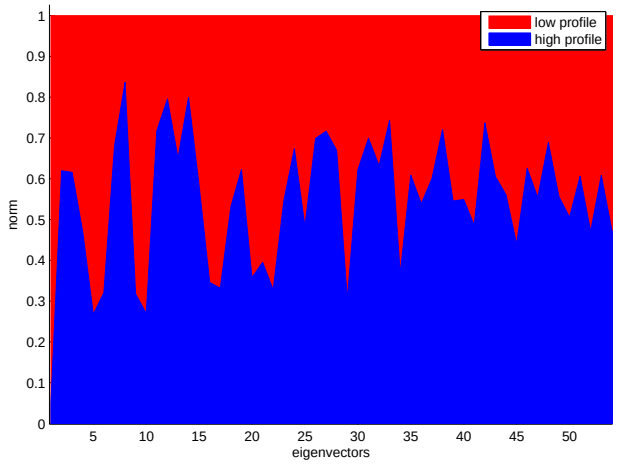

Figure 7: Norms of eigenvectors

3 CHARACTERIZATION OF DYNAMIC FORCES AT WHEEL/RAIL CONTACT

3.1 Model for the wheel-rail contact

The wheel-rail contact is studied in the orthonormal landmark of the track $(Oxyz)$, such as the vertical axle (Oz) points upward and the (Oy) axle points right. Resulting of the contact, an effort is applied to the wheel. This effort can be split into a normal force N and a tangential force T, such as

$$T \leq fN, \tag{6}$$

where f is the friction coefficient [3]. Indeed, the wheel-rail contact includes at the same time sliding and adhesion.

To model the dynamic response of the train, the equations of dynamics are solved considering the wheel-rail coupling. To study the stability and the comfort of the train, only low frequencies ($\leq$20 Hz) are of interest. That is why a multibody software is used to solve the dynamic problem. The software used in this study is Vampire. The contact is modeled with the analytical Hertz model for the normal part of the load and with the semi-analytical Kalker model for the tangential load [4]. Rather than forces N and T, their projections Y and Q in $(Oxyz)$ will be used, as shown in figure 8.

$$Q = N\cos(\delta) + T\sin(\delta) \tag{7}$$

$$Y = N\sin(\delta) - T\cos(\delta), \tag{8}$$

where δ is the angle between the contact surface and the horizontal.

The variations of contact forces trigger instability movements of the train: yaw, roll and pitch movements. While pitch and roll will be neglected in this study, the yaw, which implies an oscillation of the vehicle from right side to left side and could make the train derail, will be studied in detail. Indeed, a transversal displacement of the train triggers a change of the contact point (see figure 9). This change modifies the rolling radius and then the forces in the wheel-rail contact because of the profiled geometry of the wheel and the rail. In alignment, this phenomenon puts the axles centered on the track back. In curves, it allows the inscription of the

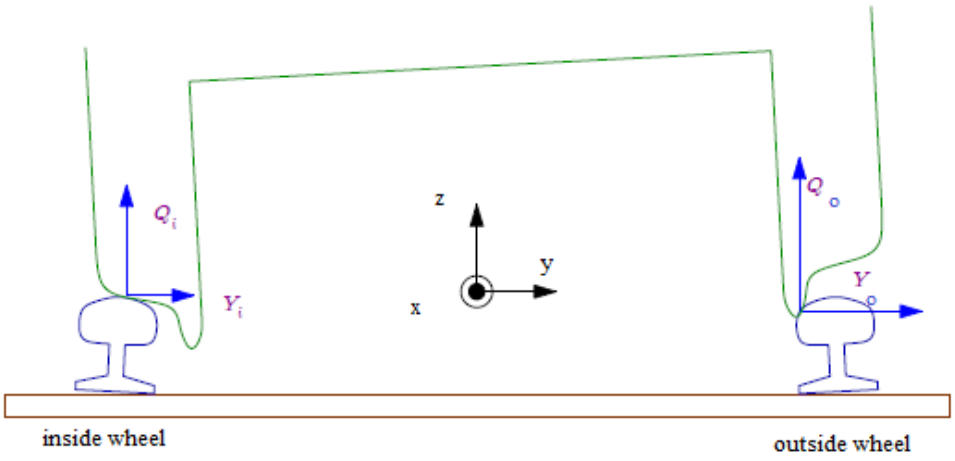

Figure 8: Forces at the wheel-rail contact

axles. That is why the wheel-rail contact can be characterized by the position of the contact and the contact angle. One can notice that the translation of the contact point along the rail profile is not continuous. There can be a gap between two contact points, and there can be two contact points at the same time.

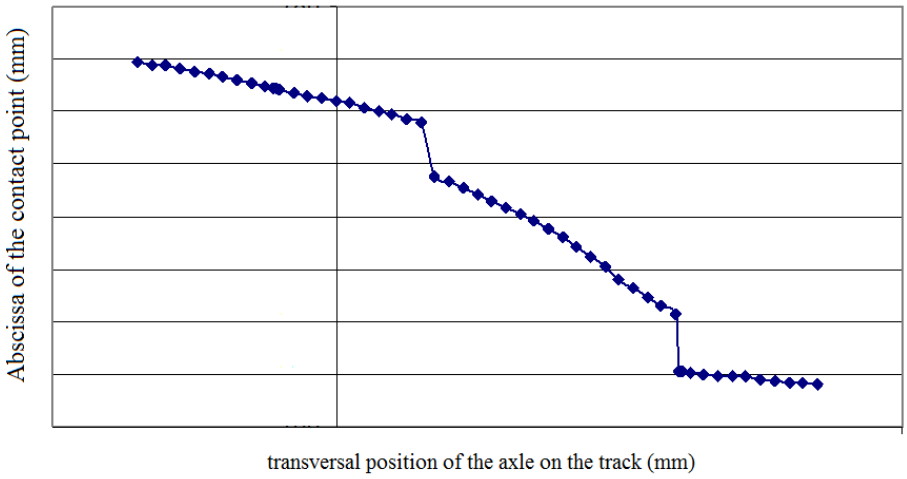

Figure 9: Lateral position of the contact point on the top of the rail

3.2 Dynamical response of the train on a new track

First, the wheel-rail contact is studied in ideal conditions (new rails, new wheels, alignment). The train used is a french Duplex TGV. Contact points are the same on the right and the left sides of the track, as shown in figure 10. There are two gaps in the contact angle and the contact position when the contact skips from the tread to the flange of the wheel. At the equilibrium, the vehicle is centered on the track. Indeed, the curves of contact positions intersect for y=0.

Then, the contact is studied with new rails and new wheels, but in a left curve of zone 4, as defined by UIC [5]. The curve radius is 282 m and the cant equals 120 mm. The goal is

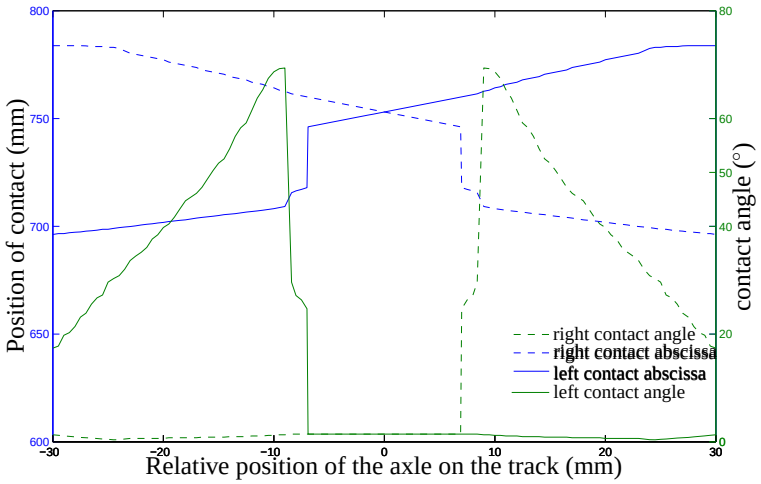

Figure 10: Ideal wheel-rail contact position and angle

to observe the train behavior in the curve (see figure 11). The train goes along the 4 km track at a speed of 70 km/h, and starts turning after 600 m. The cant deficiency in the curve is 85 mm high, and the train should deports on the right side (outside). The lateral displacement of the axles is observed in figure 12. There is a big difference between leading and trailing axles. Whereas the trailing axle moves outward, the trailing axle stays centered because it is steered by the leading axle. In particular, on the leading right wheel (on the high rail), the contact is situated on the flange and not on the tread.

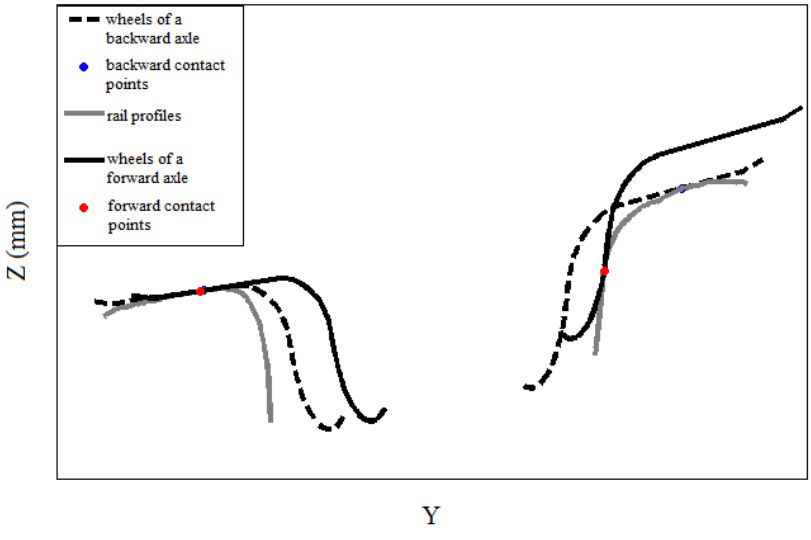

Figure 11: Wheel-rail contact in a zone 4 curve

The lateral forces applied to the axles are drawn in figure 13. For the leading axle, since the axle moves outward, the sum of lateral forces is high and inwardly directed. For the trailing axle, the sum of lateral forces is low because the axle is well centered on the track.

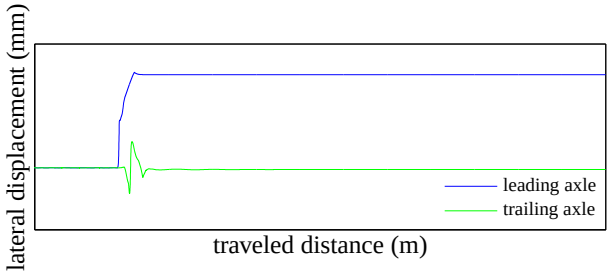

Figure 12: Lateral displacement of the axles in the curve

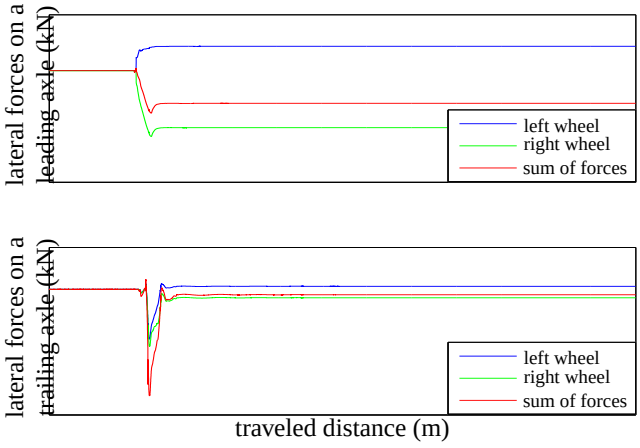

Figure 13: Lateral forces at the wheel-rail contact

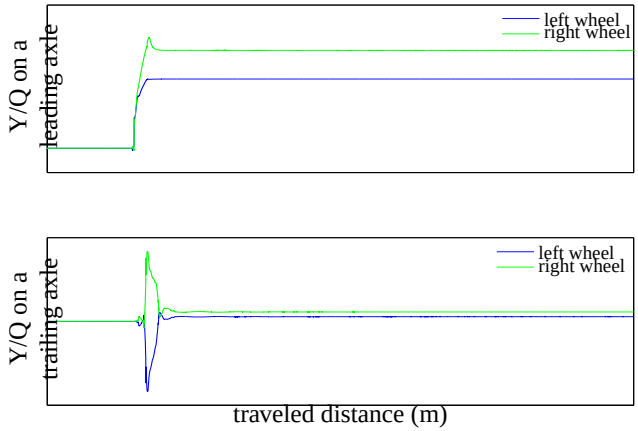

Figure 14: Quotient Y/Q at the wheel-rail contact

As a stability criteria, the quotient of lateral forces on the vertical charge Y/Q is studied in figure 14. For the leading axle, Y/Q rises in the curve, especially for the outer wheel. For the trailing axle, there is a little peak in the curve entrance, but the value stays low.

3.3 Influence of wear on train's dynamic response

Because of the friction between wheels and rails, the rails are worn in curves. Wear modifies the profile's geometry, especially in severe curves. Rail profiles are measured in a curve of zone 4, according to UIC's definition, post-processed as explained in paragraphe 2.1. One can see in figure 15 the difference between worn and new rails. The curve is the one studied in paragraph 3.2. On the high rail (right side), the rail is worn with a side-cutting wear. The low rail is used on the top of the rail. Moreover, wear introduces a gauge irregularity.

Then, the train's behavior on the measured track is computed. The static contact is deeply modified by rails' wear (see figure 16), especially on the high rail. An equilibrium position in the contact position and the contact angle disappears.

A look at the lateral displacement of the axle (see figure 17) shows no big difference betwen worn and new rails for the leading axle. The trailing axle moves inward the curve, increasing the angle between the bogie and the tangent to the track. This phenomenon might be due mostly to the gauge irregularity and not directly to the rail wear.

The lateral forces Y are then observed in figure 18. Since the position of the leading axle is almost the same as with new rails, the lateral forces on this axle have the same shape as with new rails, but around 10% higher. For the trailing axle, the lateral forces rise outward, in order to center the axle back on the track.

Figure 19 shows that the quotient Y/Q is globally the same as with new rails, but the values increase also by around 10 $\%$ in the curve, when one compares with new rails.

As a conclusion, the results show that rail wear implies a loss of stability of the train, without being insecure for the vehicle.

4 CONCLUSION AND PERSPECTIVES

This study allowed to compute the dynamic response of the train on a measured track, taking into account the rail wear. It has been seen that stability of the train decreases because of the

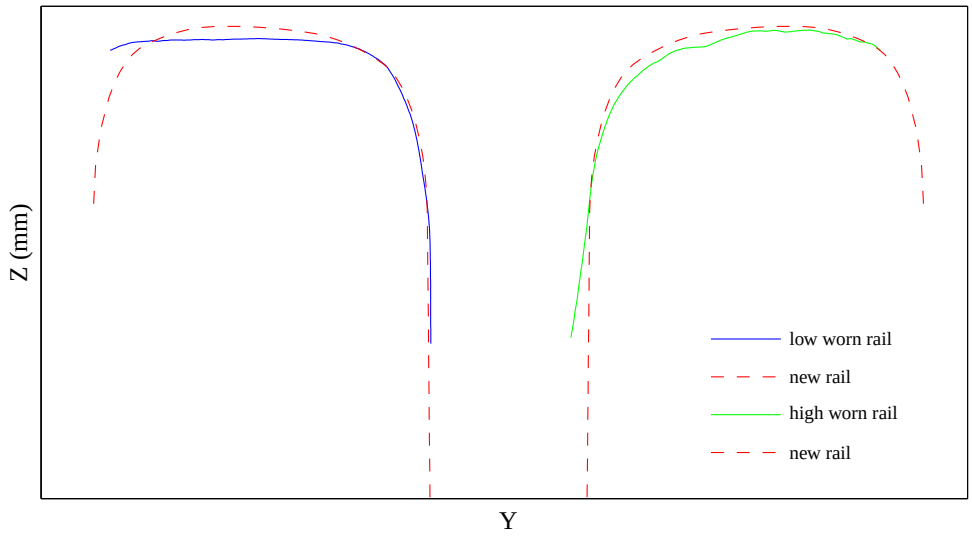

Figure 15: Measured worn rails

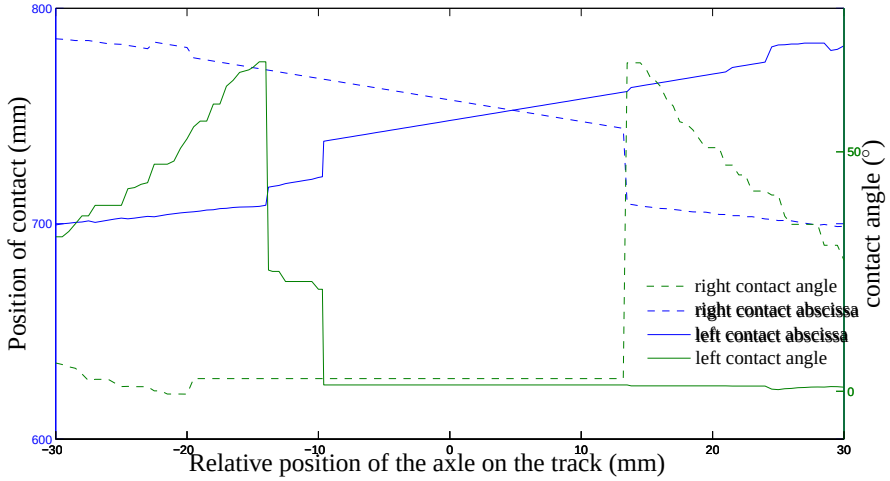

Figure 16: wheel-rail contact position and angle with worn rails

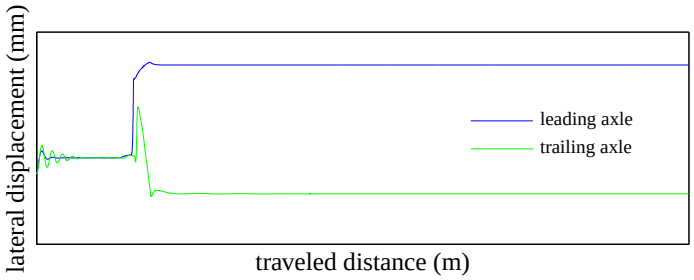

Figure 17: Lateral displacement of the axles in the curve with worn rails

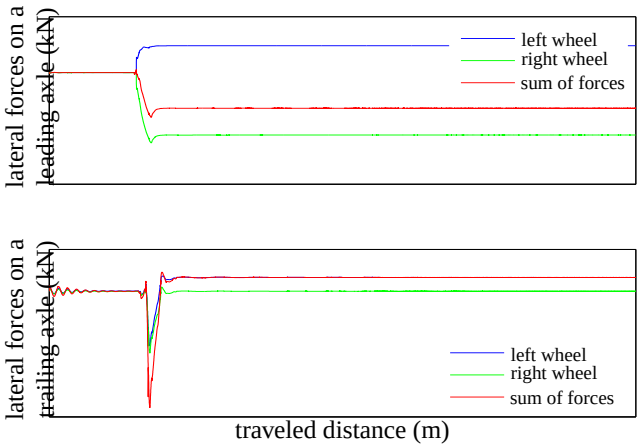

Figure 18: Lateral forces with worn rails

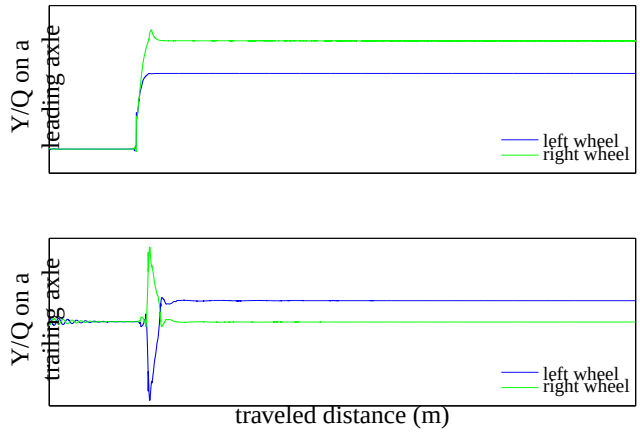

Figure 19: Quotient Y/Q with worn rails

wear, but in a small extent (around 10%). Furthermore, rail profiles have been projected on a statistical basis, in order to characterize rail wear. It has been shown that wear on high and low rails is correlated. Both rails have to be taken into account to have a representative description of the track.

Next step will consist in running a simulation of the train's behavior, using the profiles projected on the statistical basis. The dynamic response will then highlight the link between wear modes and the train stability. A statistical study will be used to characterize this dynamic response.

Acknowledgement. This work was supported by SNCF, Innovation and Research Department.

REFERENCES

[1] O.P. Le Maître, O.M. Knio, *Spectral methods for uncertainty quantification*, Springer, 2010.

[2] G. Perrin, C. Soize, D. Duhamel, C. Funfschilling, Track irregularities stochastic modeling. *Thirteenth International Conference on Civil, Structural and Environmental Engineering Computing*, Chania, Greece, 2011.

[3] B. Soua, *Etude de l'usure et de l'endommagement du roulement ferroviaire avec des modeles d'essieux non rigides*, PhD Thesis, Ecole Nationale des Ponts et Chausses, 1997.

[4] J.J. Kalker, A fast algorithm for the simplified theory of rolling contact, *Vehicle System Dynamics*, **11**, 1–13, 1982.

[5] UIC, *Leaflet 518*, October 2009.